iScience

CellPress
OPEN ACCESS

Article

Layer specific regulation of critical period timing and maturation of mouse visual cortex by endocannabinoids

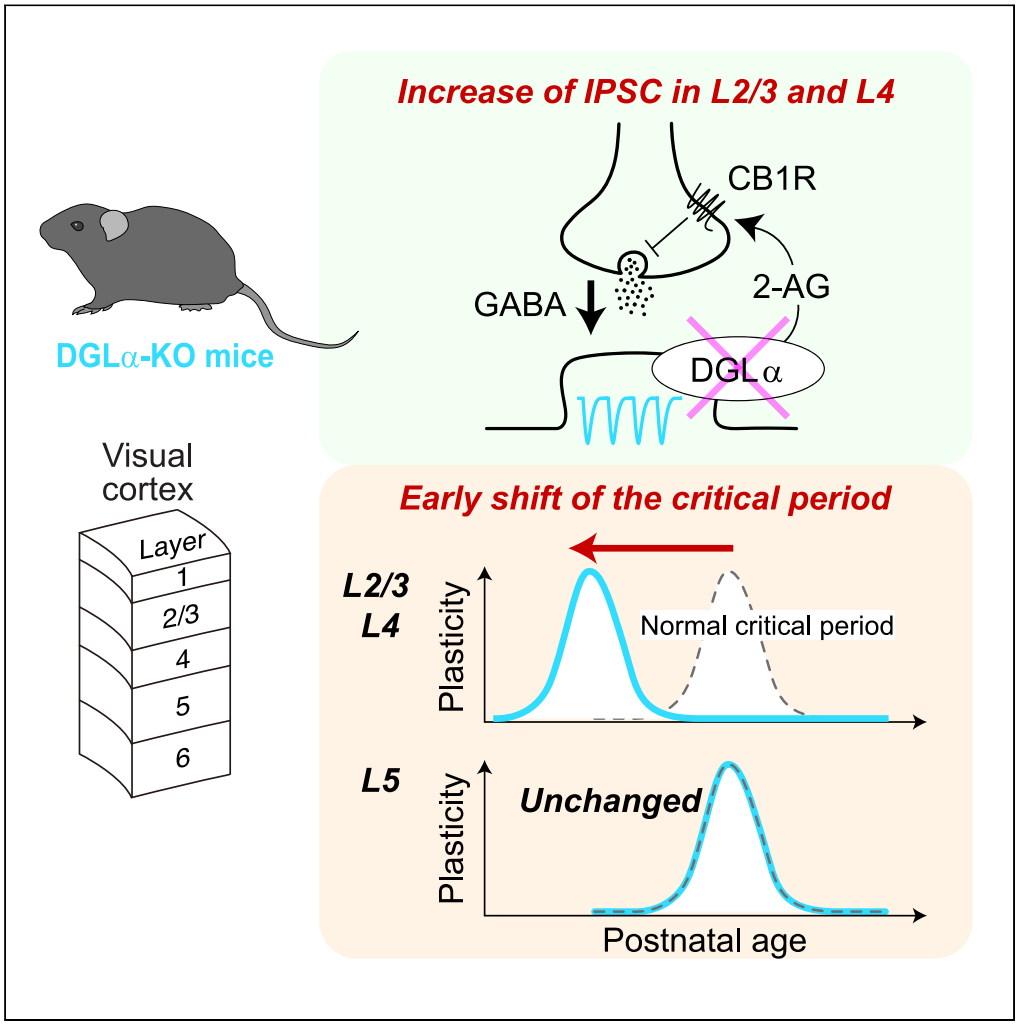

Taisuke Yoneda, Katsuro Kameyama, Takahiro Gotou, ..., Kenji Sakimura, Masanobu Kano, Yoshio Hata

yhata@tottori-u.ac.jp

Highlights

Mice lacking DGL-α exhibit precocious critical period in L2/3 and 4 of visual cortex

DGL-α KO exhibits impaired binocular matching of orientation selectivity in L2/3

DGL-α KO exhibits earlier maturation of inhibitory synaptic function in L2/3 and 4

Suppression of $GABA_A$ receptor rescues precocious ocular dominance plasticity in L4

Yoneda et al., iScience 27, 110145
June 21, 2024
https://doi.org/10.1016/j.isci.2024.110145

iScience

CellPress
OPEN ACCESS

Article

Layer specific regulation of critical period timing and maturation of mouse visual cortex by endocannabinoids

Taisuke Yoneda,[1,2,3,8] Katsuro Kameyama,[1,8] Takahiro Gotou,[1] Keiko Terata,[1] Masahiro Takagi,[2] Yumiko Yoshimura,[2,3] Kenji Sakimura,[4] Masanobu Kano,[5,6,7] and Yoshio Hata[1,9,*]

SUMMARY

Plasticity during the critical period is important for the functional maturation of cortical neurons. While characteristics of plasticity are diverse among cortical layers, it is unknown whether critical period timing is controlled by a common or unique molecular mechanism among them. We here clarified layer-specific regulation of the critical period timing of ocular dominance plasticity in the primary visual cortex. Mice lacking the endocannabinoid synthesis enzyme diacylglycerol lipase-α exhibited precocious critical period timing, earlier maturation of inhibitory synaptic function in layers 2/3 and 4, and impaired development of the binocular matching of orientation selectivity exclusively in layer 2/3. Activation of cannabinoid receptor restored ocular dominance plasticity at the normal critical period in layer 2/3. Suppression of $GABA_A$ receptor rescued precocious ocular dominance plasticity in layer 4. Therefore, endocannabinoids regulate critical period timing and maturation of visual function partly through the development of inhibitory synaptic functions in a layer-dependent manner.

INTRODUCTION

The neocortex is organized into six layers where diverse neuronal types connect to form layer-specific neural circuits and play individual roles in information processing.[1,2] Neural plasticity during a restricted period of early life, referred to as the critical period, is a fundamental mechanism for shaping precise cortical circuits. The critical period has been observed in various cortical regions, which contribute not only to sensory modalities but also to higher-order brain function.[3,4] Proper emergence of the critical period is important for the development of brain functions because mice that show abnormal critical period timing fail to develop proper neuronal functions.[5,6] In the visual system, studies have shown a causal relationship between critical period timing and functional maturation of GABAergic neural circuits.[7–9]

Ocular dominance (OD) plasticity is a well-known example of experience-dependent plasticity during the critical period in various animal species.[10–12] If one eye is occluded for several days during the critical period, neurons in the primary visual cortex (V1) lose response to the deprived eye. Several studies have shown a difference in the effect of monocular deprivation (MD) among cortical layers. The effect of MD appears faster in layer 2/3 (L2/3) than in layer 4 (L4) of kitten V1.[13] While pyramidal neurons in L2/3 and L4 clearly exhibit OD plasticity, those in layer 5 (L5) exhibit a modest change of OD in rat V1.[14] These differences in OD plasticity among cortical layers suggest that cortical plasticity was regulated by different mechanisms in each layer. However, whether the timing of the critical period is controlled by a common or unique regulatory mechanism in individual cortical layers is unclear.

The endocannabinoid (eCB) system might contribute to the layer specificity of OD plasticity, because an inverse agonist of the G protein-coupled receptor, cannabinoid receptor type 1 (CB1R), blocked OD plasticity in L2/3 but not in L4 or L5.[15,16] eCBs are lipid molecules that bind mainly to CB1R in the central nervous system. The eCB system plays a role in various aspects of neural circuit formation, such as cortical migration, axonal guidance, and synaptic plasticity.[17–20] Many *in vitro* studies have reported that eCB regulates layer-specific plasticity in excitatory and inhibitory synapses of the visual system in an age-dependent manner.[21–25] The expression of CB1R increases developmentally and distributes prominently in L2/3 and layer 6 (L6) of mouse V1.[26,27] Among known endogenous ligands of CB1R, such as anandamide and 2-arachidonoylglycerol (2-AG),[19] 2-AG is supposed to be mainly involved in synaptic plasticity[28] and also plays a crucial role in shaping

[1]Division of Neuroscience, School of Life Science, Faculty of Medicine, Tottori University, Yonago 683-8503, Japan
[2]Division of Visual Information Processing, National Institute for Physiological Sciences, Okazaki 444-8585, Japan
[3]Graduate Institute for Advanced Studies, SOKENDAI, Okazaki 444-8585, Japan
[4]Department of Animal Model Development, Brain Research Institute, Niigata University, Niigata 951-8585, Japan
[5]Department of Neurophysiology, Graduate School of Medicine, The University of Tokyo, Tokyo 113-0033, Japan
[6]International Research Center for Neurointelligence (WPI-IRCN), The University of Tokyo, Tokyo 113-0033, Japan
[7]Advanced Comprehensive Research Organization (ACRO), Teikyo University, Tokyo 173-0003, Japan
[8]These authors contributed equally
[9]Lead contact
*Correspondence: yhata@tottori-u.ac.jp
https://doi.org/10.1016/j.isci.2024.110145

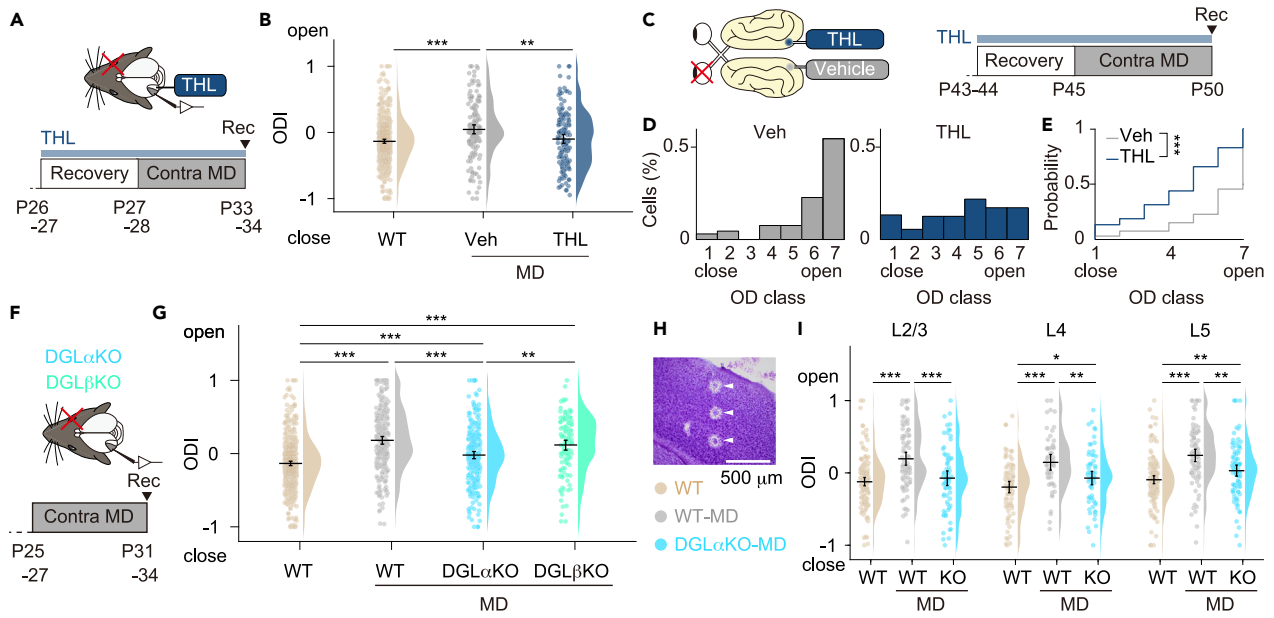

Figure 1. DGLα contributes to OD plasticity in a layer-specific manner

(A) The left hemisphere of mouse V1 was continuously infused with THL, an inhibitor of DGL, using an osmotic pump. After recovery from pump implantation, the right eye was deprived of vision for 6 days. Neuronal activity in V1 was recorded from the left hemisphere.

(B) Raincloud plots show the OD distribution of nondeprived wild-type mice (WT, n = 530 units in 12 mice), vehicle-treated MD mice (Veh-MD, n = 153 units in 4 mice), and THL-treated MD mice (THL-MD, n = 161 units in 4 mice). Pale colored circles indicate ODIs of individual spiking units. Clouds show kernel density estimation of ODI distribution. The black horizontal bar and error bars indicate mean ODI and 95% confidence interval (CI) calculated using bias-corrected and accelerated bootstrap methods, respectively. Negative and positive ODIs represent response preferences to deprived and nondeprived eyes, respectively.

(C) THL was administered to kittens. THL or vehicle solution was continuously infused by an osmotic pump to the right or left hemisphere of kitten V1, respectively. The left eye was deprived for 5 days. Neuronal activity was obtained from both hemispheres.

(D) OD histograms were obtained from vehicle-treated (Veh, n = 66 units) and THL-treated (THL, n = 128 units) hemispheres of kittens (n = 2). OD classes 1 and 7 indicate proportions of neurons only responding to deprived and nondeprived eyes, respectively. Neurons in class 4 respond equally to both eyes.

(E) Cumulative representation of OD distribution in THL- and vehicle-treated groups in (D).

(F) MD was performed for 6–7 days in DGLα and β KO mice. Following MD, visual responses were recorded from contralateral V1 to the deprived eye.

(G) The distribution of ODIs in nondeprived wild-type mice (same data as in (B), monocularly deprived wild-type mice (WT-MD, n = 259 units in 6 mice), DGLα-KO mice (DGLαKO-MD, n = 261 units in 7 mice), and DGLβ-KO mice (DGLβKO-MD, n = 124 units in 4 mice).

(H) Electric lesions (arrowheads) were made along an electrode track to locate recording sites in Nissl-stained coronal sections.

(I) Raincloud plots show the OD distribution in each layer of three mouse groups at P32 (WT, n = 140 (L2/3), 86 (L4), and 150 (L5) units in 9 mice; WT-MD, n = 87 (L2/3), 52 (L4), and 86 (L5) units in 6 mice; DGLαKO-MD, n = 73 (L2/3), 67 (L4), and 97 (L5) units in 7 mice). Permutation test with Holm–Bonferroni method was conducted in (B), (G) and (I), and Kolmogorov-Smirnov test was performed in (E) (*$p < 0.05$, **$p < 0.01$, ***$p < 0.001$).

See also Figure S1.

thalamocortical projections in developing cortex.[29] 2-AG is synthesized by the combined action of phospholipase C and diacylglycerol lipase (DGL), which has two isoforms DGLα and DGLβ.[30,31] In the central nervous system, DGLα richly expresses at postsynaptic site[32,33] and produces 2-AG that retrogradely binds to presynaptic CB1R and induces the suppression of neurotransmitter release.[28,34] In the visual system, CB1R was reported to regulate OD plasticity in L2/3;[15] however, whether DGL is involved in layer-specific regulation of OD plasticity has not been demonstrated. In addition, the relationship between the eCB system and critical period timing is totally unknown.

In this study, we examined the role of the eCB system in OD plasticity. We found that deletion of DGLα accelerated critical period timing in L2/3 and L4 of mouse V1. Precocious critical period timing observed in DGLα knockout mice was mediated by the altered functional maturation of inhibitory synapses. Thus, our results collectively indicate that the DGLα–2-AG–CB1R system regulates the critical period timing of mouse V1 in a layer-specific manner.

RESULTS

Diacylglycerol lipase α regulates ocular dominance plasticity in a layer-specific manner

To evaluate the involvement of 2-AG in OD plasticity, we blocked the synthesis of 2-AG pharmacologically by infusing an inhibitor of DGLα and β, tetrahydrolipstatin (THL), into one hemisphere of V1 in C57BL/6 mice at postnatal days 26–27 (P26–P27) (Figure 1A). The contralateral eye was deprived of vision for 6 days in the critical period. The effect of MD was examined by extracellular recording in the binocular region of V1. Neuronal activity was sorted into single-unit responses, and an OD index (ODI) was calculated for each of them. We note that the infusion

of THL did not affect the neuronal activity of V1. The magnitude of spontaneous and evoked activity, and response specificity such as OD and orientation selectivity were not altered by THL in nondeprived mice (Figures S1A–S1D). Consistent with the results of another study,[35] ODI distribution was biased to the contralateral eye in wild-type (WT) mice (Figure 1B). MD shifted OD to the ipsilateral open eye in the vehicle-applied group (Figure 1B, $p < 0.001$, Hedges' $g = 0.482$). The infusion of THL disrupted this OD shift (Figure 1B, vehicle vs. THL, $p < 0.01$, $g = 0.339$). In addition, the disruption of OD plasticity by THL was confirmed in monocularly deprived cats (Figures 1C–1E). Thus, the contribution of 2-AG in OD plasticity is a common feature across species.

To determine which synthetic enzyme of 2-AG, DGLα or DGLβ contributes to OD plasticity, we examined the effect of MD in DGLα/β-KO mice (Figure 1F). In the DGLα-KO mice 2-AG level in the brain is reduced to about 20% of WT mice, while in the DGLβ-KO mice it is comparable to WT mice.[28] MD for 6–7 days caused a significant OD shift in WT mice (Figure 1G, $p < 0.001$, $g = 0.832$). Similarly, monocularly deprived DGLβ-KO mice demonstrated a significant shift of OD ($p < 0.001$, $g = 0.700$), which was comparable with that of monocularly deprived WT mice ($p = 0.163$, $g = 0.152$). By contrast, the ODI distribution of monocularly deprived DGLα-KO mice was significantly different from both nondeprived ($p < 0.001$, $g = 0.308$) and deprived WT mice ($p < 0.001$, $g = 0.486$). OD distribution in nondeprived DGLα-KO mice was similar to WT mice (Figure S1E). Thus, DGLα but not DGLβ partially contributes to OD plasticity.

We analyzed OD plasticity in individual cortical layers to examine whether OD plasticity was disrupted in a subset of neurons in DGLα-KO mice (Figure 1H). MD induced significant OD shift in every layer in WT mice at P32 (Figure 1I, L2/3, $g = 0.828$; L4, $g = 0.894$; L5, $g = 0.924$; $p < 0.001$ in every layer). OD distribution in nondeprived DGLα-KO mice was similar to WT mice in every layer (Figure S1E). OD plasticity in deprived DGLα-KO mice was completely inhibited in L2/3 and ODI was comparable with that of nondeprived WT mice (Figure 1I, KO-MD vs. WT-MD, $p < 0.001$, $g = 0.615$; KO-MD vs. WT, $p = 0.373$, $g = 0.130$). By contrast, L4 and L5 of DGLα-KO mice exhibited a mild change in OD because the ODIs were significantly different for both deprived (L4, $g = 0.554$; L5, $g = 0.542$; $p < 0.01$ in both layers) and nondeprived (L4, $p < 0.05$, $g = 0.331$; L5, $p < 0.01$, $g = 0.353$) WT mice. Hence, DGLα contributes to OD plasticity more strongly in L2/3 than in L4 and L5 of V1.

Precocious ocular dominance plasticity and binocular mismatching of visual responses in the upper layer of diacylglycerol lipase α-KO mice

Our results indicate that DGLα is involved in OD plasticity in a layer-specific manner. We next examined its contribution to critical period timing in each cortical layer. Because age dependency of OD plasticity in individual layers has not been fully evaluated in mice, we first examined the degree of OD plasticity before the peak of a critical period in WT mice. We performed MD for 4 days starting from P13 and P17 (Figure 2A). MD for P13–P17 exerted no significant effect on OD in any layer (Figure 2A, left column, L2/3, $p = 0.231$, $g = 0.166$; L4, $p = 0.411$, $g = 0.139$; L5, $p = 0.720$, $g = 0.037$). Following MD for P17–P21, we found a significant OD shift in L2/3 and L5, but the OD shift was less pronounced in L4 (Figure 2A, middle column, L2/3, $p < 0.001$, $g = 0.580$; L4, $p = 0.090$, $g = 0.230$; L5, $p < 0.001$, $g = 0.513$). Later MD starting from P26 induced a significant OD shift in L4. These results may be relevant to other reports that extragranular cells are more sensitive to MD than cells in L4.[13,36]

In DGLα-KO mice, MD for P17–P21 induced a significant OD shift in L2/3 and L5 as observed in WT mice (Figure 2A, middle column, L2/3, $p < 0.001$, $g = 0.548$; L5, $p < 0.01$, $g = 0.364$). In L4, we found a significant OD shift compared with both nondeprived ($p < 0.001$, $g = 0.589$) and deprived WT mice ($p < 0.05$, $g = 0.353$). These results indicate that DGLα-KO mice exhibit OD plasticity before the normal critical period. Furthermore, MD for P13–P17 induced a significant OD shift in L2/3 of DGLα-KO mice, but not in L4 and L5 (Figure 2A, left column, L2/3, $p < 0.05$, $g = 0.341$; L4, $p = 0.571$, $g = 0.084$; L5, $p = 0.440$, $g = 0.078$). Thus, the absence of eCB signaling leads to earlier critical period onset in L2/3 and L4.

Correct timing of the critical period is necessary for the proper development of visual function.[5,6,37] To evaluate whether the precocious timing of the critical period in DGLα-KO mice affects the maturation of visual function, we compared the binocular matching of orientation preference between WT and DGLα-KO mice at P34–P36. The preferred orientations of individual V1 neurons were determined for two eyes independently presenting grating stimuli in 12 directions and the degree of mismatch between them was evaluated (Figure 2B). The mismatch of preferred orientations was prominent in L2/3, modest in L4, and not significant in L5 between DGLα-KO and WT mice (Figure 2C, L2/3, $p < 0.05$, $g = 0.479$; L4, $p = 0.176$, $g = 0.257$; L5, $p = 0.599$, $g = 0.098$). Thus, DGLα-KO mice show the abnormal development of binocular vision accompanied by the precocious timing of the critical period in L2/3 of V1.

Developmental changes in the distribution and expression of diacylglycerol lipase α

We examined the distribution of DGLα in the visual cortex of developing WT mice. At P30, DGLα immunoreactivity was denser in the binocular region of V1 than in the monocular region and medial V2 ($p < 0.001$) (Figures 3A and 3B). DGLα was mainly present in L2/3 and L4, and CB1R was rich in the upper parts of L2/3 and L6[26,27] (Figure 3C). At a finer structure level, consistent with the spatial restriction of synaptic regulation by eCBs,[38] DGLα-immunopositive particles were located within 20 μm around CB1R-immunopositive boutons (Figures S2A–S2C).

Regarding developmental changes of DGLα expression in WT mice, the level of DGLα protein increased significantly after P30 compared with P10 (Figures 3D, 3E, and S2D, $p < 0.01$), with a peak at P40. The intense immunoreactivity of DGLα in L2/3 and L4 appeared clearly after P30 (Figures 3F and 3G, $p < 0.001$) and the laminar pattern did not change thereafter. Considering that DGLα-KO mice have exhibited precocious critical period, the developmental increase of DGLα may slow the timing of the critical period.

We also performed immunostaining for CB1R and $GABA_A$ receptors in DGLα-KO mice to address whether the knockout of DGLα affects the expression of other proteins, which could potentially account for the precocious OD plasticity. The results showed that at P17, when OD plasticity is observed in DGLα-KO mice, we observed a significant expression of DGLα in WT mice compared to DGLα-KO mice (Figure S2E).

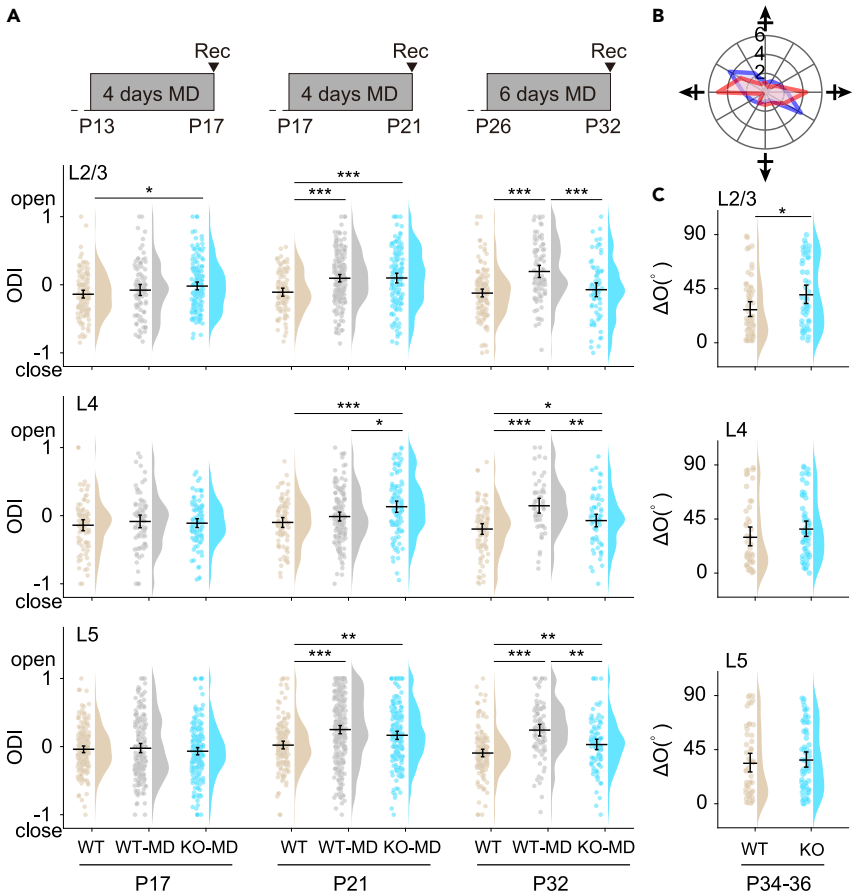

Figure 2. DGLα controls the critical period timing and binocular correspondence of preferred orientations in a layer-specific manner

(A) The effect of MD was examined at P17, P21, and P32 following 4 or 6 days of MD. Raincloud plots show the OD distribution in each layer of three mouse groups at different ages. Data of P32 animals are taken from Figure 1I. P17: wild-type (WT), n = 121 (L2/3), 86 (L4), and 183 (L5) units in 6 mice; wild-type MD (WT-MD), n = 94 (L2/3), 76 (L4), and 174 (L5) units in 5 mice; DGLα-KO-MD (KO-MD), n = 163 (L2/3), 97 (L4), and 209 (L5) units in 6 mice. P21: WT, n = 99 (L2/3), 86 (L4), and 157 (L5) units in 5 mice; WT-MD, n = 187 (L2/3), 145 (L4), and 255 (L5) units in 8 mice; KO-MD, n = 140 (L2/3), 105 (L4), and 189 (L5) units in 6 mice.

(B) An example of the orientation preference of a V1 neuron. The radial coordinate represents response amplitude (spikes/s) to grating visual stimuli in a particular direction indicated around the chart. Responses to contralateral (blue) and ipsilateral (red) eyes to the recording hemispheres are plotted. The preferred orientation differs slightly between the two eyes in this case.

(C) Layer breakdown of the angular difference of the preferred orientation in wild-type and DGLα-KO mice (WT, n = 60 (L2/3), 50 (L4), and 52 (L5) units in 8 mice; DGLα-KO, n = 51 (L2/3), 61 (L4), and 68 (L5) units in 8 mice). Permutation test with Holm–Bonferroni method was performed in (A) and (C) (*$p < 0.05$, **$p < 0.01$, ***$p < 0.001$).

However, there was no significant difference in the expression of CB1R and $GABA_A$ receptors in each cortical layer between DGLα-KO and WT mice (Figures S2F and S2G).

Inhibition contributes to precocious critical period timing in diacylglycerol lipase α-KO mice

To elucidate the regulatory mechanism of the precocious critical period timing in DGLα-KO mice, we examined the development of inhibitory synaptic function in each layer. We recorded miniature inhibitory postsynaptic currents (mIPSCs) in L2/3 and L4 pyramidal neurons of P17, P21, and P26 mice using whole-cell patch-clamp recording of brain slices (Figures 4A and 4B). In WT mice, mIPSC frequency increased through development both in L2/3 and L4 (Figure 4C, L2/3, P17 vs. P21, $p < 0.01$, $g = 0.865$, P17 vs. P26, $p < 0.001$, $g = 2.431$; L4, P17 vs. P21, $p < 0.001$, $g = 2.214$, P17 vs. P26, $p < 0.001$, $g = 3.660$), whereas the amplitude remained unchanged (Figure 4D, L2/3, P17 vs. P21, $p = 0.336$, $g = 0.297$, P17 vs. P26, $p = 0.100$, $g = 0.529$; L4, P17 vs. P21, $p = 0.954$, $g = 0.018$, P17 vs. P26, $p = 0.466$, $g = 0.220$), consistent with the results of another study.[39] In L2/3 of DGLα-KO mice, mIPSC frequency increased at P17 and decreased at P26 compared with WT mice (Figure 4C, L2/3, P17, $p < 0.01$, $g = 0.896$; P26, $p < 0.05$, $g = 1.023$). mIPSC frequency increased at both P17 and P21 in L4 of DGLα-KO mice (Figure 4C, L4, P17, $p < 0.01$, $g = 1.037$; P21, $p < 0.05$, $g = 0.856$). By contrast, no significant difference was observed in mIPSC amplitude between DGLα-KO and WT mice (Figure 4D, L2/3, P17, $p = 0.499$, $g = 0.176$, P21, $p = 0.72$, $g = 0.121$, P26, $p = 0.856$, $g = 0.07$; L4, P17, $p = 0.453$, $g = 0.212$, P21, $p = 0.463$, $g = 0.239$, P26, $p = 0.829$, $g = 0.077$). Although the mIPSCs of DGLα-KO mice showed slower rise time both in L2/3

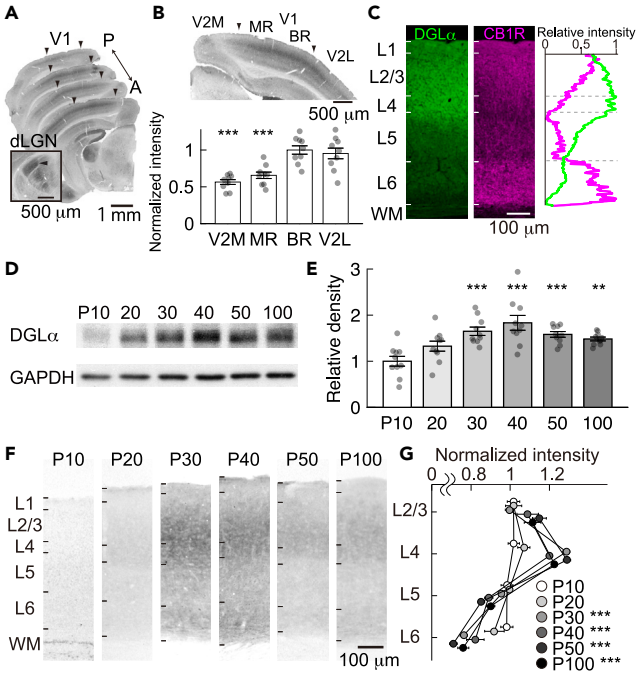

Figure 3. Developmental change in the layer distribution and expression of DGLα in mouse V1

(A) Coronal sections of P30 mice were immunostained for DGLα. Four sections from anterior ("A") to posterior ("P") are displayed. Arrowheads indicate the boundaries between V1 and V2. Inset shows a representative image of the dorsal lateral geniculate nucleus (dLGN, arrowhead) immunostained for DGLα.

(B) Top: Distribution of DGLα in the visual cortex (V2M: medial extrastriate area, V2L: lateral extrastriate area, MR: monocular region in V1, BR: binocular region in V1). Bottom: Signal intensity of DGLα immunoreactivity in L2/3 of each cortical region (n = 9 ROIs in 3 mice; bars, mean; error bars, SEM). The signal intensities are normalized to that in BR (one-way ANOVA, $p < 0.001$; Dunnett's post hoc test, ***$p < 0.001$ compared with the intensity in BR).

(C) Coronal sections of V1 at P30 immunostained for DGLα and CB1R. In the graph on the right, green and magenta lines show the intensity profiles of DGLα and CB1R immunoreactivity along the cortical depth, respectively.

(D) Representative western blots showing DGLα and GAPDH expression in V1 at various postnatal ages.

(E) Relative densities of western blot bands for DGLα are plotted at various ages (n = 10 hemispheres in 5 mice for each age; bars, mean; error bars, SEM). Band densities are normalized to the density at P10 (one-way ANOVA, $p < 0.001$; Dunnett's post hoc test, **$p < 0.01$, ***$p < 0.001$ compared with density at P10).

(F) Representative sections of the binocular region of V1 immunostained for DGLα at various postnatal ages.

(G) Intensity profiles of DGLα immunoreactivity in individual layers at various ages. The intensity in each layer is normalized to the average of all layers at each age. (n = 4–5 mice for each age; error bars, SEM, one-way ANOVA, ***$p < 0.001$).

See also Figure S2.

and L4 at P17, their half-widths were comparable with those of WT mice (Figures S3A and S3B). Administration of AM251, a CB1R inverse agonist, significantly increased mIPSC frequency both in L2/3 at P17 and L4 at P21 in WT mice but not in DGLα-KO mice indicating that a loss of CB1R-mediated signaling underlies the increase of mIPSC frequency in DGLα-KO mice (Figures S3C and S3D). These results indicate that the DGLα–2-AG–CB1R pathway regulates the developmental upregulation of inhibitory synaptic function.

We examined the causal relationship between inhibitory function and the precocious critical period timing in DGLα-KO mice. We administered methyl 6,7-dimethoxy-4-ethyl-β-carboline-3-carboxylate (DMCM), an inverse agonist of $GABA_A$ receptor, to DGLα-KO mice during MD (Figure 4E). First, we have confirmed that DMCM administration itself does not affect OD in non-deprived DGLα-KO mice (Figure S3E). Although MD at P17–P21 induces a significant OD shift in L4 of DGLα-KO but not in WT mice (Figure 2A), OD shift in L4 was abolished in DMCM-treated DGLα-KO mice (Figure 4F, $p < 0.001$, $g = 0.522$) and OD distribution was comparable with that of WT mice (Figure 2A, WT-MD of P21, $p = 0.212$, $g = 0.166$). On the other hand, we found no difference in OD distribution between control and DMCM-treated mice in L2/3 and L5 (Figure 4F, L2/3; $p = 0.463$, $g = 0.102$; L5, $p = 0.129$, $g = 0.144$; All, $p < 0.01$, $g = 0.163$). Thus, DMCM treatment has suppressed precocious OD shift but did not further suppress the OD shift that was also seen in WT mice. Therefore, an increase in GABAergic inputs would be required for precocious OD plasticity in L4 of DGLα-KO mice. In L2/3, on the other hand, DMCM treatment did not disturb the precocious OD plasticity following MD at P13-P17 (Figure 4G, All, $p = 0.464$, $g = 0.046$; L2/3, $p = 0.700$, $g = 0.048$; L4, $p = 0.936$, $g = 0.014$; L5, $p = 0.093$, $g = 0.172$).

Activation of cannabinoid receptors rescues ocular dominance plasticity in L2/3 of diacylglycerol lipase α-KO mice

We finally investigated whether a cannabinoid receptor (CBR) agonist, WIN 55, 212-2 (WIN), could rescue OD plasticity in DGLα-KO mice at the critical period (Figure 4H). Acute administration of WIN to 4-week-old mice induced a significant reduction in the amplitude of

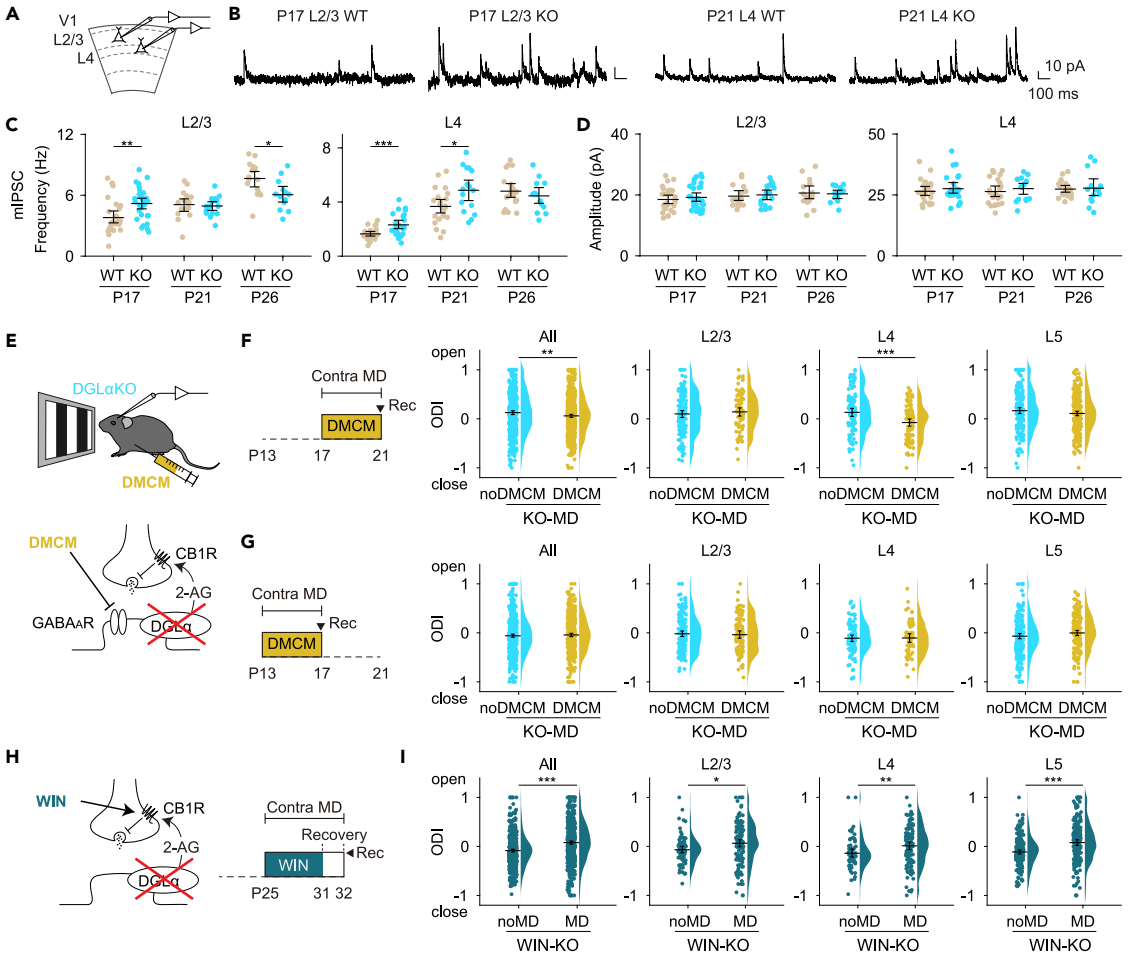

Figure 4. Measurement of inhibitory synaptic transmission in slice preparations and effects of drug administration on OD plasticity in DGLα-KO mice

(A) Whole-cell patch-clamp recording was performed in L2/3 and L4 pyramidal neurons in mouse V1 slices.

(B) Representative mIPSC traces from L2/3 (P17) and L4 (P21) in wild-type and DGLα-KO mice.

(C and D) mIPSC frequency (C) and amplitude (D) in L2/3 (WT, n = 28 (P17), 17 (P21), and 16 (P26) cells; KO, n = 31 (P17), 17 (P21), and 13 (P26) cells) and in L4 (WT, n = 25 (P17), 23 (P21), and 21 (P26) cells; KO, n = 25 (P17), 16 (P21), and 14 (P26) cells). Colored circles show data from individual cells. The black horizontal bar and error bars indicate mean and 95% CI, respectively.

(E) DMCM, an inverse agonist of the $GABA_A$ receptor, was intraperitoneally injected into DGLα-KO mice during MD until 9 hours before the recording.

(F) DMCM treatment was performed at P17-P21. Raincloud plots show the OD distribution after MD in nontreated (noDMCM, n = 482 (all), the same data as P21 KO-MD in Figure 2A) and DMCM-treated DGLα-KO mice (DMCM, n = 619 (all), 79 (L2/3), 91 (L4), and 266 (L5) units in 6 mice).

(G) DMCM treatment was performed at P13-P17. Raincloud plots show the OD distribution after MD in nontreated (noDMCM, n = 526 (all), the same data as P17 KO-MD in Figure 2A) and DMCM-treated DGLα-KO mice (DMCM, n = 473 (all), 96 (L2/3), 60 (L4), and 186 (L5) units in 6 mice).

(H) A cannabinoid receptor agonist, WIN was injected into DGLα-KO mice intraperitoneally during MD until the day before the recording experiment.

(I) OD distributions of WIN-treated DGLα-KO mice without MD (noMD, n = 498 (all), 81 (L2/3), 66 (L4), and 203 (L5) units in 5 mice) and with MD (MD, n = 589 (all), 133 (L2/3), 114 (L4), and 201 (L5) units in 6 mice). Permutation test was performed in (C), (D), (F), (G) and (I) (*$p < 0.05$, **$p < 0.01$, ***$p < 0.001$).

See also Figure S3.

visually evoked field potential (VEP) (Figures S3F–S3H). We next chronically administered WIN to DGLα-KO mice for P25-P31. The WIN administration itself did not affect OD distribution in DGLα-KO mice (KO in Figure S1E vs. WIN KO noMD in Figure 4I, All, $p = 0.284$, $g = 0.106$; L2/3, $p = 0.073$, $g = 0.369$; L4, $p = 0.676$, $g = 0.092$; L5, $p = 0.225$, $g = 0.178$). Comparison of the ODIs between WIN-treated DGLα-KO mice with and without MD showed significant OD plasticity in every layer in the MD mice (Figure 4I, All, $p < 0.001$, $g = 0.446$; L2/3, $p < 0.05$, $g = 0.349$; L4, $p < 0.01$, $g = 0.402$; L5, $p < 0.001$, $g = 0.531$). As mentioned above, OD plasticity was observed in L4 and L5 even in DGLα-KO mice without WIN administration (Figure 1I), and the degree of OD plasticity was not influenced by WIN administration (KO-MD in Figure 1I vs. WIN KO-MD in Figure 4I, L4, $p = 0.168$, $g = 0.211$; L5, $p = 0.334$, $g = 0.120$). Therefore, WIN administration would have restored OD plasticity in L2/3 but did not further enhance the OD shift in L4 and L5 of DGLα-KO mice at this postnatal age.

DISCUSSION

We demonstrated that the eCB system controls the critical period onset of OD plasticity partly through the functional maturation of inhibitory synapses. A deficit of DGLα induced precocious OD plasticity and upregulated inhibitory synaptic function before the critical period in L2/3 and L4, and disrupted the maturation of binocular matching of orientation preference in L2/3 of V1. Activation of CB1R restored OD plasticity at the normal critical period in L2/3. Suppression of $GABA_A$ receptor rescued precocious OD plasticity in L4 in DGLα-KO mice.

An inverse agonist of CB1R was reported to inhibit OD plasticity in L2/3 at the critical period.[15] 2-AG synthesized by DGLα has been shown to mediate eCB-dependent synaptic modulation.[28,34,40] Our results revealed that a deficit of DGLα but not DGLβ impaired OD plasticity in L2/3 at P26, and the administration of a CBR agonist rescued OD plasticity in L2/3 of DGLα-KO mice. Consistent with the physiological results, DGLα was detected mainly in the lower part of L2/3 and L4, and CB1R was observed in the upper part of L2/3 in developing V1.[26] Thus, the DGLα–2-AG–CB1R signaling cascade is important for OD plasticity in L2/3 at the critical period of WT mice.

DGLα-KO mice demonstrated OD plasticity at a younger age than WT mice. Precocious critical period has been reported in some mice lines,[6,41,42] which show two common features: accelerated maturation of GABA function[6,42] and loss of binocular matching of orientation preference.[5,6] An increase in GABA function has been reported to accelerate critical period onset.[8,43,44] Consistent with these results, DGLα-KO mice showed an increase in mIPSC frequency earlier than WT mice and decreased level of binocular matching of orientation preference. In addition, an inverse agonist of the $GABA_A$ receptor suppressed precocious plasticity in L4. Thus, the eCB system controls critical period timing through the development of inhibitory neuronal circuits in L4 and contributes to the functional maturation of V1 neurons.

In L2/3, DGLα-KO mice at P17 showed precocious OD plasticity and an increase in mIPSC frequency in pyramidal neurons. A CB1R blocker increased mIPSC frequency in WT mice but not in DGLα-KO mice. Consistently, a CBR agonist was reported to depress the magnitude of evoked IPSC in L2/3 in 1–3-week-old WT mice.[45] The eCB signal may suppress inhibitory transmission at P17. A high expression level of CB1R at inhibitory terminals in the upper layer supports this hypothesis anatomically.[26] Thus, the DGLα–CB1R signaling pathway controls inhibitory synaptic function in L2/3 at 2 weeks of age. However, the attempt to weaken inhibitory function through DMCM administration did not suppress precocious OD plasticity. Therefore, the precocious OD plasticity in L2/3 at this age may not be due to an enhancement of inhibitory function. However, it should be noted that the effect of DMCM treatment in this experiment may have been somewhat limited at P13-P17 compared to P17-P21. DMCM acts on the benzodiazepine binding site of $GABA_A$ receptors and the amount of this binding in the visual cortex of rats increases sharply from P9 to P25.[46] At the same period, $GABA_A$ receptor α1 subunit with high benzodiazepine affinity increases.[47,48] Therefore, we cannot exclude the possibility that the DMCM treatment did not sufficiently weaken the inhibitory function at P13-P17. Consequently, we cannot make a definitive statement about the involvement of altered inhibitory function in precocious OD plasticity in L2/3 at this age.

In L4, DGLα-KO mice exhibited an increase in mIPSC frequency at P17 and P21 and precocious OD plasticity. A CB1R inverse agonist increased mIPSC frequency in WT mice, and a pharmacological weakening of $GABA_A$ receptor function suppressed precocious OD plasticity in DGLα-KO mice. Thus, eCB modulates inhibitory synaptic function, thereby regulating the onset of the critical period in L4. By contrast, a CBR agonist reportedly did not affect the amplitude and frequency of spontaneous IPSC or the amplitude of evoked IPSC in L4 at P21.[25,45] These results may reflect the saturation of CBR function in the inhibitory synapses of WT mice.

At 4 weeks of age, L2/3 pyramidal neurons in DGLα-KO mice exhibited lower mIPSC frequency than WT mice, suggesting a weakening of cortical inhibitory function. In addition, a CBR agonist recovered disrupted OD plasticity in L2/3. At this age, excitatory synapses, but not inhibitory synapses, were reported to be CB1R-sensitive in L2/3.[22,45] We found a decrease in VEP amplitude after the application of the CBR agonist, which is consistent with previous findings that a CB1R blocker increases VEP amplitude.[15] Kainate-induced seizures are suppressed by the augmentation of 2-AG levels and enhanced by CBR antagonists.[49] Therefore, the activation of the DGLα-CBR pathway would downregulate visual cortical excitability at 4 weeks of age. In this study, the impairment of OD plasticity in DGLα-KO mice at P26 may reflect the reduced cortical excitability, which could differ from the termination mechanism of the critical period in WT mice, and the CBR agonist might have adjusted the excitatory–inhibitory balance to recover OD plasticity in L2/3.[50] Alternatively, it might be due to a lack of the molecular mechanism that drives OD plasticity, since an inverse agonist of CB1R inhibits OD plasticity at this age.[15,16] By contrast, in L4, the restorative effect of the CBR agonist was not significant. This is consistent with previous findings that a CB1R inverse agonist does not affect the plasticity of excitatory synapses or OD plasticity in L4.[15,16,22]

In L5, a deficit of DGLα did not affect critical period onset and binocular matching. Thus, L5 neurons should have eCB-independent regulatory mechanisms for critical period timing. However, we found an attenuation of OD plasticity in L5 of DGLα-KO mice. The partial contribution of eCB to OD plasticity in L5 neurons may be because eCB modulates synaptic transmission and plasticity in a subset of L5 neurons.[51–53]

Among inhibitory neuronal subtypes, the maturation of parvalbumin (PV)-expressing interneurons is believed to regulate critical period onset.[6,42,54] Although CB1R exists rarely in PV neurons, CB1R-sensitive unitary IPSCs were detected between PV and pyramidal neurons in the visual cortex.[24,55,56] Hence, the lack of eCB signaling in some PV neurons may promote inhibitory transmission and accelerate critical period onset. Furthermore, CB1R is abundantly expressed in cholecystokinin-positive inhibitory neurons that show eCB-sensitive inhibitory synaptic transmission.[52,57–59] In mouse V1, the neuronal activity of cholecystokinin-positive inhibitory neurons, which have little PV expression, is modulated by the cortical state and visual input.[60] Thus, the lack of eCB might have altered cortical activity pattern and influenced critical period onset.

Limitations of the study

In the experiments to determine whether the enhancement of inhibitory transmission participates in the precocious OD plasticity, DMCM administration could not affect the precocious OD plasticity in L2/3 at P13-P17. Because the effectiveness of DMCM

administration is not certain at P13-17 as described in the Discussion, we could not reach a conclusion about the involvement of altered inhibitory function in the precocious OD plasticity in L2/3 at this age. This is a limitation of pharmacological experiment *in vivo* in which it is difficult to evaluate the effects of administered drugs. In the present study, we have discussed primarily about neurons, but CB receptors distribute on both neurons and glial cells. Thus, we cannot rule out the possibility that the reduction of 2-AG in DGLα-KO mice might have affected endocannabinoid signaling in glial cells and been involved in altered OD plasticity.

STAR★METHODS

Detailed methods are provided in the online version of this paper and include the following:

- KEY RESOURCES TABLE
- RESOURCE AVAILABILITY
  - Lead contact
  - Materials availability
  - Data and code availability
- EXPERIMENTAL MODEL AND STUDY PARTICIPANT DETAILS
  - Animals
- METHOD DETAILS
  - Drug administration
  - Monocular deprivation
  - Electrophysiological recording in mice
  - Electrophysiological recording in cats
  - Nissl staining
  - Western blotting
  - Immunostaining
  - Slice electrophysiology
  - Data analysis for *in vivo* electrophysiology
  - Image analysis
  - Subcellular localization of DGLα and CB1R
  - VEP recording for WIN administered mice
- QUANTIFICATION AND STATISTICAL ANALYSIS
  - Statistics

SUPPLEMENTAL INFORMATION

Supplemental information can be found online at https://doi.org/10.1016/j.isci.2024.110145.

ACKNOWLEDGMENTS

We thank Masahiko Watanabe (Hokkaido University) for providing DGLα antibody. We thank K. Esumi, Y. Daimyo, Y. Mitsui, M. Nakanishi, K. Ishigami, S. Omura, and M. Higa for assistance regarding experiments. We thank previous and current members of the laboratory for helpful discussions. This work was supported by KAKENHI (21K06431) and Takeda Science Foundation to T.Y, KAKENHI (18K06523 and 24K14273) to Y.H. This study was supported by the Cooperative Study Program (20-117, 21-116, 22NIPS128, 23NIPS126, 24NIPS140) of National Institute for Physiological Sciences.

AUTHOR CONTRIBUTIONS

T.Y., K.K., and Y.H. designed research; T.Y., K.K., T.G., K.T., M.T., Y.Y., K.S., M.K., and Y.H. performed research; T.Y., K.K., T.G., M.T., and Y.Y. analyzed data; and T.Y., K.K., and Y.H. wrote the article.

DECLARATION OF INTERESTS

The authors declare no competing interests.

Received: May 25, 2023
Revised: April 15, 2024
Accepted: May 27, 2024
Published: May 29, 2024

REFERENCES

1. Douglas, R.J., and Martin, K.A.C. (2004). Neuronal circuits of the neocortex. Annu. Rev. Neurosci. *27*, 419–451. https://doi.org/10.1146/annurev.neuro.27.070203.144152.
2. Harris, K.D., and Mrsic-Flogel, T.D. (2013). Cortical connectivity and sensory coding. Nature *503*, 51–58. https://doi.org/10.1038/nature12654.
3. Hensch, T.K. (2004). Critical period regulation. Annu. Rev. Neurosci. *27*, 549–579. https://doi.org/10.1146/annurev.neuro.27.070203.144327.
4. Chakraborty, R., Vijay Kumar, M.J., and Clement, J.P. (2021). Critical aspects of neurodevelopment. Neurobiol. Learn. Mem. *180*, 107415. https://doi.org/10.1016/j.nlm.2021.107415.
5. Wang, B.S., Feng, L., Liu, M., Liu, X., and Cang, J. (2013). Environmental enrichment rescues binocular matching of orientation preference in mice that have a precocious critical period. Neuron *80*, 198–209. https://doi.org/10.1016/j.neuron.2013.07.023.
6. Krishnan, K., Wang, B.S., Lu, J., Wang, L., Maffei, A., Cang, J., and Huang, Z.J. (2015). MeCP2 regulates the timing of critical period plasticity that shapes functional connectivity in primary visual cortex. Proc. Natl. Acad. Sci. USA *112*, E4782–E4791. https://doi.org/10.1073/pnas.1506499112.
7. Hensch, T.K., Fagiolini, M., Mataga, N., Stryker, M.P., Baekkeskov, S., and Kash, S.F. (1998). Local GABA circuit control of experience-dependent plasticity in developing visual cortex. Science *282*, 1504–1508. https://doi.org/10.1126/science.282.5393.1504.
8. Fagiolini, M., and Hensch, T.K. (2000). Inhibitory threshold for critical-period activation in primary visual cortex. Nature *404*, 183–186. https://doi.org/10.1038/35004582.
9. Hensch, T.K. (2005). Critical period plasticity in local cortical circuits. Nat. Rev. Neurosci. *6*, 877–888. https://doi.org/10.1038/nrn1787.
10. Wiesel, T.N., and Hubel, D.H. (1963). Single-cell responses in striate cortex of kittens deprived of vision in one eye. J. Neurophysiol. *26*, 1003–1017. https://doi.org/10.1152/jn.1963.26.6.1003.
11. Dräger, U.C. (1978). Observations on monocular deprivation in mice. J. Neurophysiol. *41*, 28–42. https://doi.org/10.1152/jn.1978.41.1.28.
12. Hubel, D.H., Wiesel, T.N., and LeVay, S. (1977). Plasticity of ocular dominance columns in monkey striate cortex. Philos. Trans. R. Soc. Lond. B Biol. Sci. *278*, 377–409. https://doi.org/10.1098/rstb.1977.0050.
13. Trachtenberg, J.T., Trepel, C., and Stryker, M.P. (2000). Rapid extragranular plasticity in the absence of thalamocortical plasticity in the developing primary visual cortex. Science *287*, 2029–2032. https://doi.org/10.1126/science.287.5460.2029.
14. Medini, P. (2011). Layer- and cell-type-specific subthreshold and suprathreshold effects of long-term monocular deprivation in rat visual cortex. J. Neurosci. *31*, 17134–17148. https://doi.org/10.1523/jneurosci.2951-11.2011.
15. Liu, C.H., Heynen, A.J., Shuler, M.G.H., and Bear, M.F. (2008). Cannabinoid receptor blockade reveals parallel plasticity mechanisms in different layers of mouse visual cortex. Neuron *58*, 340–345. https://doi.org/10.1016/j.neuron.2008.02.020.
16. Frantz, M.G., Crouse, E.C., Sokhadze, G., Ikrar, T., Stephany, C.É., Nguyen, C., Xu, X., and McGee, A.W. (2020). Layer 4 gates plasticity in visual cortex independent of a canonical microcircuit. Curr. Biol. *30*, 2962–2973.e5. https://doi.org/10.1016/j.cub.2020.05.067.
17. Berghuis, P., Rajnicek, A.M., Morozov, Y.M., Ross, R.A., Mulder, J., Urbán, G.M., Monory, K., Marsicano, G., Matteoli, M., Canty, A., et al. (2007). Hardwiring the brain: Endocannabinoids shape neuronal connectivity. Science *316*, 1212–1216. https://doi.org/10.1126/science.1137406.
18. Mulder, J., Aguado, T., Keimpema, E., Barabás, K., Ballester Rosado, C.J., Nguyen, L., Monory, K., Marsicano, G., Di Marzo, V., Hurd, Y.L., et al. (2008). Endocannabinoid signaling controls pyramidal cell specification and long-range axon patterning. Proc. Natl. Acad. Sci. USA *105*, 8760–8765. https://doi.org/10.1073/pnas.0803545105.
19. Kano, M., Ohno-Shosaku, T., Hashimotodani, Y., Uchigashima, M., and Watanabe, M. (2009). Endocannabinoid-mediated control of synaptic transmission. Physiol. Rev. *89*, 309–380. https://doi.org/10.1152/physrev.00019.2008.
20. Itami, C., Huang, J.Y., Yamasaki, M., Watanabe, M., Lu, H.C., and Kimura, F. (2016). Developmental switch in spike timing-dependent plasticity and cannabinoid-dependent reorganization of the thalamocortical projection in the barrel cortex. J. Neurosci. *36*, 7039–7054. https://doi.org/10.1523/jneurosci.4280-15.2016.
21. Sjöström, P.J., Turrigiano, G.G., and Nelson, S.B. (2003). Neocortical LTD via coincident activation of presynaptic NMDA and cannabinoid receptors. Neuron *39*, 641–654. https://doi.org/10.1016/s0896-6273(03)00476-8.
22. Crozier, R.A., Wang, Y., Liu, C.H., and Bear, M.F. (2007). Deprivation-induced synaptic depression by distinct mechanisms in different layers of mouse visual cortex. Proc. Natl. Acad. Sci. USA *104*, 1383–1388. https://doi.org/10.1073/pnas.0609596104.
23. Huang, Y., Yasuda, H., Sarihi, A., and Tsumoto, T. (2008). Roles of endocannabinoids in heterosynaptic long-term depression of excitatory synaptic transmission in visual cortex of young mice. J. Neurosci. *28*, 7074–7083. https://doi.org/10.1523/jneurosci.0899-08.2008.
24. Jiang, B., Huang, S., de Pasquale, R., Millman, D., Song, L., Lee, H.K., Tsumoto, T., and Kirkwood, A. (2010). The maturation of GABAergic transmission in visual cortex requires endocannabinoid-mediated LTD of inhibitory inputs during a critical period. Neuron *66*, 248–259. https://doi.org/10.1016/j.neuron.2010.03.021.
25. Garkun, Y., and Maffei, A. (2014). Cannabinoid-dependent potentiation of inhibition at eye opening in mouse V1. Front. Cell. Neurosci. *8*, 46. https://doi.org/10.3389/fncel.2014.00046.
26. Yoneda, T., Kameyama, K., Esumi, K., Daimyo, Y., Watanabe, M., and Hata, Y. (2013). Developmental and visual input-dependent regulation of the CB1 cannabinoid receptor in the mouse visual cortex. PLoS One *8*, e53082. https://doi.org/10.1371/journal.pone.0053082.
27. Koukouli, F., Montmerle, M., Aguirre, A., De Brito Van Velze, M., Peixoto, J., Choudhary, V., Varilh, M., Julio-Kalajzic, F., Allene, C., Mendéz, P., et al. (2022). Visual-area-specific tonic modulation of GABA release by endocannabinoids sets the activity and coordination of neocortical principal neurons. Cell Rep. *40*, 111202. https://doi.org/10.1016/j.celrep.2022.111202.
28. Tanimura, A., Yamazaki, M., Hashimotodani, Y., Uchigashima, M., Kawata, S., Abe, M., Kita, Y., Hashimoto, K., Shimizu, T., Watanabe, M., et al. (2010). The endocannabinoid 2-arachidonoylglycerol produced by diacylglycerol lipase α mediates retrograde suppression of synaptic transmission. Neuron *65*, 320–327. https://doi.org/10.1016/j.neuron.2010.01.021.
29. Itami, C., Uesaka, N., Huang, J.Y., Lu, H.C., Sakimura, K., Kano, M., and Kimura, F. (2022). Endocannabinoid-dependent formation of columnar axonal projection in the mouse cerebral cortex. Proc. Natl. Acad. Sci. USA *119*, e2122700119. https://doi.org/10.1073/pnas.2122700119.
30. Stella, N., Schweitzer, P., and Piomelli, D. (1997). A second endogenous cannabinoid that modulates long-term potentiation. Nature *388*, 773–778. https://doi.org/10.1038/42015.
31. Bisogno, T., Howell, F., Williams, G., Minassi, A., Cascio, M.G., Ligresti, A., Matias, I., Schiano-Moriello, A., Paul, P., Williams, E.J., et al. (2003). Cloning of the first sn1-DAG lipases points to the spatial and temporal regulation of endocannabinoid signaling in the brain. J. Cell Biol. *163*, 463–468. https://doi.org/10.1083/jcb.200305129.
32. Yoshida, T., Fukaya, M., Uchigashima, M., Miura, E., Kamiya, H., Kano, M., and Watanabe, M. (2006). Localization of diacylglycerol lipase-α around postsynaptic spine suggests close proximity between production site of an endocannabinoid, 2-arachidonoyl-glycerol, and presynaptic cannabinoid CB1 receptor. J. Neurosci. *26*, 4740–4751. https://doi.org/10.1523/jneurosci.0054-06.2006.
33. Uchigashima, M., Narushima, M., Fukaya, M., Katona, I., Kano, M., and Watanabe, M. (2007). Subcellular arrangement of molecules for 2-arachidonoyl-glycerol-mediated retrograde signaling and its physiological contribution to synaptic modulation in the striatum. J. Neurosci. *27*, 3663–3676. https://doi.org/10.1523/jneurosci.0448-07.2007.
34. Gao, Y., Vasilyev, D.V., Goncalves, M.B., Howell, F.V., Hobbs, C., Reisenberg, M., Shen, R., Zhang, M.Y., Strassle, B.W., Lu, P., et al. (2010). Loss of retrograde endocannabinoid signaling and reduced adult neurogenesis in diacylglycerol lipase knock-out mice. J. Neurosci. *30*, 2017–2024. https://doi.org/10.1523/jneurosci.5693-09.2010.
35. Gordon, J.A., and Stryker, M.P. (1996). Experience-dependent plasticity of binocular responses in the primary visual cortex of the mouse. J. Neurosci. *16*, 3274–3286. https://doi.org/10.1523/jneurosci.16-10-03274.1996.
36. Daw, N.W., Fox, K., Sato, H., and Czepita, D. (1992). Critical period for monocular deprivation in the cat visual cortex. J. Neurophysiol. *67*, 197–202. https://doi.org/10.1152/jn.1992.67.1.197.
37. Wang, B.S., Sarnaik, R., and Cang, J. (2010). Critical period plasticity matches binocular orientation preference in the visual cortex.

Neuron *65*, 246–256. https://doi.org/10.1016/j.neuron.2010.01.002.

38. Wilson, R.I., and Nicoll, R.A. (2001). Endogenous cannabinoids mediate retrograde signalling at hippocampal synapses. Nature *410*, 588–592. https://doi.org/10.1038/35069076.
39. Tatti, R., Swanson, O.K., Lee, M.S.E., and Maffei, A. (2017). Layer-specific developmental changes in excitation and inhibition in rat primary visual cortex. eNeuro *4*, e0402-17. https://doi.org/10.1523/eneuro.0402-17.2017.
40. Yoshino, H., Miyamae, T., Hansen, G., Zambrowicz, B., Flynn, M., Pedicord, D., Blat, Y., Westphal, R.S., Zaczek, R., Lewis, D.A., and Gonzalez-Burgos, G. (2011). Postsynaptic diacylglycerol lipase mediates retrograde endocannabinoid suppression of inhibition in mouse prefrontal cortex. J. Physiol. *589*, 4857–4884. https://doi.org/10.1113/jphysiol.2011.212225.
41. Hanover, J.L., Huang, Z.J., Tonegawa, S., and Stryker, M.P. (1999). Brain-derived neurotrophic factor overexpression induces precocious critical period in mouse visual cortex. J. Neurosci. *19*, RC40. https://doi.org/10.1523/jneurosci.19-22-j0003.1999.
42. Huang, Z.J., Kirkwood, A., Pizzorusso, T., Porciatti, V., Morales, B., Bear, M.F., Maffei, L., and Tonegawa, S. (1999). BDNF regulates the maturation of inhibition and the critical period of plasticity in mouse visual cortex. Cell *98*, 739–755. https://doi.org/10.1016/s0092-8674(00)81509-3.
43. Iwai, Y., Fagiolini, M., Obata, K., and Hensch, T.K. (2003). Rapid critical period induction by tonic inhibition in visual cortex. J. Neurosci. *23*, 6695–6702. https://doi.org/10.1523/jneurosci.23-17-06695.2003.
44. Fagiolini, M., Fritschy, J.M., Löw, K., Möhler, H., Rudolph, U., and Hensch, T.K. (2004). Specific $GABA_A$ circuits for visual cortical plasticity. Science *303*, 1681–1683. https://doi.org/10.1126/science.1091032.
45. Jiang, B., Sohya, K., Sarihi, A., Yanagawa, Y., and Tsumoto, T. (2010). Laminar-specific maturation of GABAergic transmission and susceptibility to visual deprivation are related to endocannabinoid sensitivity in mouse visual cortex. J. Neurosci. *30*, 14261–14272. https://doi.org/10.1523/jneurosci.2979-10.2010.
46. Schliebs, R., Rothe, T., and Bigl, V. (1986). Dark-rearing affects the development of benzodiazepine receptors in the central visual structures of rat brain. Brain Res. *389*, 179–185. https://doi.org/10.1016/0165-3806(86)90185-9.
47. Lüddens, H., and Wisden, W. (1991). Function and pharmacology of multiple $GABA_A$ receptor subunits. Trends Pharmacol. Sci. *12*, 49–51. https://doi.org/10.1016/0165-6147(91)90495-E.
48. Laurie, D.J., Wisden, W., and Seeburg, P.H. (1992). The distribution of thirteen $GABA_A$ receptor subunit mRNAs in the rat brain. III. Embryonic and postnatal development. J. Neurosci. *12*, 4151–4172. https://doi.org/10.1523/JNEUROSCI.12-11-04151.1992.
49. Sugaya, Y., Yamazaki, M., Uchigashima, M., Kobayashi, K., Watanabe, M., Sakimura, K., and Kano, M. (2016). Crucial roles of the endocannabinoid 2-arachidonoylglycerol in the suppression of epileptic seizures. Cell Rep. *16*, 1405–1415. https://doi.org/10.1016/j.celrep.2016.06.083.
50. Morishita, H., and Hensch, T.K. (2008). Critical period revisited: impact on vision. Curr. Opin. Neurobiol. *18*, 101–107. https://doi.org/10.1016/j.conb.2008.05.009.
51. Díaz-Alonso, J., Guzmán, M., and Galve-Roperh, I. (2012). Endocannabinoids via CB_1 receptors act as neurogenic niche cues during cortical development. Philos. Trans. R. Soc. Lond. B Biol. Sci. *367*, 3229–3241. https://doi.org/10.1098/rstb.2011.0385.
52. Bodor, Á.L., Katona, I., Nyíri, G., Mackie, K., Ledent, C., Hájos, N., and Freund, T.F. (2005). Endocannabinoid signaling in rat somatosensory cortex: Laminar differences and involvement of specific interneuron types. J. Neurosci. *25*, 6845–6856. https://doi.org/10.1523/jneurosci.0442-05.2005.
53. Varga, C., Lee, S.Y., and Soltesz, I. (2010). Target-selective GABAergic control of entorhinal cortex output. Nat. Neurosci. *13*, 822–824. https://doi.org/10.1038/nn.2570.
54. Sugiyama, S., Di Nardo, A.A., Aizawa, S., Matsuo, I., Volovitch, M., Prochiantz, A., and Hensch, T.K. (2008). Experience-dependent transfer of Otx2 homeoprotein into the visual cortex activates postnatal plasticity. Cell *134*, 508–520. https://doi.org/10.1016/j.cell.2008.05.054.
55. Sun, W., Wang, L., Li, S., Tie, X., and Jiang, B. (2015). Layer-specific endocannabinoid-mediated long-term depression of GABAergic neurotransmission onto principal neurons in mouse visual cortex. Eur. J. Neurosci. *42*, 1952–1965. https://doi.org/10.1111/ejn.12958.
56. Huang, S., and Kirkwood, A. (2020). Endocannabinoid signaling contributes to experience-induced increase of synaptic release sites from parvalbumin interneurons in mouse visual cortex. Front. Cell. Neurosci. *14*, 571133. https://doi.org/10.3389/fncel.2020.571133.
57. Katona, I., Sperlágh, B., Sík, A., Käfalvi, A., Vizi, E.S., Mackie, K., and Freund, T.F. (1999). Presynaptically located CB1 cannabinoid receptors regulate GABA release from axon terminals of specific hippocampal interneurons. J. Neurosci. *19*, 4544–4558. https://doi.org/10.1523/jneurosci.19-11-04544.1999.
58. Marsicano, G., and Lutz, B. (1999). Expression of the cannabinoid receptor CB1 in distinct neuronal subpopulations in the adult mouse forebrain. Eur. J. Neurosci. *11*, 4213–4225. https://doi.org/10.1046/j.1460-9568.1999.00847.x.
59. Tsou, K., Mackie, K., Sañudo-Peña, M.C., and Walker, J.M. (1999). Cannabinoid CB1 receptors are localized primarily on cholecystokinin-containing GABAergic interneurons in the rat hippocampal formation. Neuroscience *93*, 969–975. https://doi.org/10.1016/s0306-4522(99)00086-x.
60. Bugeon, S., Duffield, J., Dipoppa, M., Ritoux, A., Prankerd, I., Nicoloutsopoulos, D., Orme, D., Shinn, M., Peng, H., Forrest, H., et al. (2022). A transcriptomic axis predicts state modulation of cortical interneurons. Nature *607*, 330–338. https://doi.org/10.1038/s41586-022-04915-7.
61. Kuramoto, E., Furuta, T., Nakamura, K.C., Unzai, T., Hioki, H., and Kaneko, T. (2009). Two types of thalamocortical projections from the motor thalamic nuclei of the rat: a single neuron-tracing study using viral vectors. Cereb. Cortex *19*, 2065–2077. https://doi.org/10.1093/cercor/bhn231.

STAR★METHODS

KEY RESOURCES TABLE

REAGENT or RESOURCE	SOURCE	IDENTIFIER
Antibodies		
Rabbit polyclonal anti-DGLα	Frontier Institute	RRID: AB_2571691
Rabbit polyclonal anti-CB1	Frontier Institute	RRID: AB_2571591
Goat polyclonal anti-CB1	Frontier Institute	RRID: AB_2571592
Guinea pig polyclonal anti-CB1	Frontier Institute	RRID: AB_2571593
Mouse monoclonal anti-GAPDH	Merck	RRID: AB_2107445
Donkey HRP anti-rabbit IgG	GE Healthcare	RRID: AB_772206
Rabbit polyclonal anti-$GABA_AR$ α1	Frontier Institute	RRID: AB_2571571
Sheep HRP anti-mouse IgG	GE Healthcare	RRID: AB_772210
Goat biotinylated anti-rabbit IgG	Vector Laboratories	RRID: AB_2313606
Donkey Alexa Fluor 488 anti-rabbi IgG	Thermo Fisher Scientific	RRID: AB_2535792
Donkey Alexa Fluor 568 anti-goat IgG	Thermo Fisher Scientific	RRID: AB_2534104
Goat Alexa Fluor 488 anti-rabbit IgG	Thermo Fisher Scientific	RRID: AB_2576217
Goat Alexa Fluor 555 anti-rabbit IgG	Thermo Fisher Scientific	RRID: AB_2535851
Goat Alexa Fluor 647 anti-guinea pig IgG	Thermo Fisher Scientific	RRID: AB_2735091
Chemicals, peptides, and recombinant proteins		
Tetrahydrolipstatin	Merck	Item# O4139; CAS: 96829-58-2
WIN 55, 212-2	Cayman Chemical	Item# 10009023; CAS: 131543-23-2
DMCM	Tocris Bioscience	Item# 3083; CAS: 1215833-62-7
AM251	Cayman Chemical	Item#; 71670 CAS: 183232-66-8
Tetrodotoxin citrate	LATOXAN	Item# L8502; CAS: 18660-81-6
D-AP5	abcam	Item# ab120003; CAS: 79055-68-8
NBQX	abcam	Item# ab120046; CAS: 479347-86-9
Experimental models: Organisms/strains		
Mouse: DGLα knockout mice	Tanimura et al., 2010[28]	N/A
Mouse: DGLβ knockout mice	Tanimura et al., 2010[28]	N/A
Software and algorithms		
ImageJ	NIH	https://imagej.nih.gov/ij/
Offline Sorter	Plexon	https://plexon.com/products/offline-sorter/
NeuroExplorer	Nex Technologies	http://www.neuroexplorer.com/
MATLAB	MathWorks	https://jp.mathworks.com/products/matlab.html
SPSS	IBM	https://www.ibm.com/analytics/data-science/predictive-analytics/spss-statistical-software
Mini Analysis	Synaptosoft	http://bluecell.co.kr/theme/theme05/product/product_02_01.php
pCLAMP10	Molecular devices	https://www.moleculardevices.co.jp/systems/pclamp-11-software-suite#Resources

RESOURCE AVAILABILITY

Lead contact

Further information and requests for resources and reagents should be directed to and will be fulfilled by the lead contact, Yoshio Hata (yhata@tottori-u.ac.jp (Y.H.)).

Materials availability

This study did not generate new materials.

Data and code availability

- All data supporting the findings of this study will be shared by the lead contact Yoshio Hata upon request.
- This paper does not report original code.
- Any additional information required to reanalyze the data reported in this work is available from the lead contact upon request.

EXPERIMENTAL MODEL AND STUDY PARTICIPANT DETAILS

Animals

We used wild-type, homozygous DGLα- and DGLβ-KO[28] C57BL/6 mice at postnatal day (P)10–P100. Both male and female animals were used. Genotyping of the mice was performed for each animal by PCR of tail DNA samples. Cats at P43–P50 were obtained in the breeding colony of the Tottori University Advanced Medicine & Translational Research Center. This study was performed under the approval of the Animal Care and Use Committee of Tottori University (Approval number: 15-Y-19, 18-Y-15, 21-Y-13) and the National Institutes of Natural Sciences (Approval number: 19A050).

METHOD DETAILS

Drug administration

For administration of tetrahydrolipstatin (THL, O4139, Merck), animals were anesthetized with 0.5–4% isoflurane in N_2O and O_2 (1:1). A 30G stainless steel cannula connected to an osmotic minipump (ALZET 1007D, Durect) was inserted into one side of mouse V1 (0 mm anterior to the lambda, 2.5 mm to the midline, and 0.5 mm in depth from the cortical surface). The cannula was fixed to the skull by a light-cured resin composite (UniFil Flow, GC). THL was dissolved in Ringer's solution with 50% DMSO (10 mM) and filled in the osmotic pump. In cats, osmotic minipumps (ALZET 2002, Durect) were implanted into both hemispheres (3 mm posterior to the ear position, 2 mm to the midline, and 2 mm in depth from the cortical surface). The pump on one side contained the THL solution, and the pump on the other side contained the vehicle solution. All solutions were infused continuously at 0.5 μl/h.

For application of a CBR agonist, WIN 55, 212-2 (WIN) (10009023, Cayman Chemical) was dissolved at the concentration of 0.25 mg/ml in saline with 20% DMSO and 10% Tween 80. The WIN solution was injected intraperitoneally (5 mg/kg) under anesthesia with isoflurane. WIN was given every 12 hours for 6 days until the day before the recording experiment.

For treatment with an inverse agonist of $GABA_A$ receptors, DMCM (3083, Tocris Bioscience) was injected intraperitoneally (1.0 mg/kg in saline). DMCM was administered every 8 hours for 4 days until 9 hours before the recordings.

Monocular deprivation

Animals were anesthetized with 0.5-4.0% isoflurane in N_2O and O_2 (1:1). One eye was deprived of vision by eyelid suture. The sutured eyelids were treated with antibacterial ointment (Ofloxin, TOA Pharmaceuticals). The incisions were infiltrated with lidocaine (Xylocaine jelly, AstraZeneca). Lid closure was checked daily.

Electrophysiological recording in mice

Mice were anesthetized by an intraperitoneal injection of 25 mg/kg sodium pentobarbital after a preanesthetic injection of chlorprothixene (0.2 mg/mouse, i.m.), supplemented with additional doses of sodium pentobarbital when necessary. Atropine (0.3 mg/kg, s.c.) and dexamethasone (2.0 mg/kg, s.c.) were administered as preanesthetic drugs. The incisions were infiltrated with lidocaine. Contact lenses were placed on the corneas. The heart rate was monitored continuously, and body temperature was kept at 37.0–37.5°C using a heating pad (NS-TC10, Neuroscience). A craniotomy was performed over the binocular region of V1, contralateral to the deprived eye.

Extracellular recording was performed with a tungsten microelectrode (4–10 MΩ; FHC). The microelectrode was inserted in V1 with a hydraulic micromanipulator (MO-8-W, NARISHIGE), and the depth from the cortical surface was recorded. Signals were amplified and filtered with an AC amplifier (0.3–5 kHz; Model 1800, A-M Systems) and monitored using an oscilloscope (VC-11, Nihon Kohden) and an audio monitor (AM10, Grass Instruments). To sample neurons at similar locations on the visual field, we first moved electrodes from lateral to medial on V1 and located the visual field center. Recordings were performed over three penetrations in each mouse, taking care to keep the distribution of receptive fields similar among animals and within 20° at most in azimuth. After identifying receptive fields for each eye using hand-held light stimuli, activity was digitized at a sampling rate of 40 kHz and stored in a computer (MAP System, Plexon). Moving square-wave gratings

(spatial frequency, 0.05 cycle/degree; temporal frequency, 2 Hz) were presented on a display, which was placed 25-cm away from the eyes. The stimuli were presented three times alternatively to each eye and moved in 8 directions each for 2.0 s to measure OD or 12 directions each for 1.5 s to measure binocular correspondence. Spontaneous activity was measured during presentation of a blank screen. At the end of each penetration, electrolytic lesions were produced to determine the recording sites. A negative current (1 μA for 10 s) was applied through the microelectrode at two or three positions along the length of the penetration.

Electrophysiological recording in cats

Cats were sedated with medetomidine, given buprenorphine hydrochloride (0.02 mg/kg i.m., Lepetan, Otsuka) for analgesia. Then they were anesthetized with 4–5% isoflurane in N_2O and O_2 (1:1) and maintained with sodium pentobarbital (2–4 mg/kg/h, i.v.). The pupils were dilated with 0.5% tropicamide and 0.5% phenylephrine hydrochloride (Mydrin-P, Santen Pharmaceutical), and contact lenses were placed on the corneas. The animals were paralyzed with pancuronium bromide (0.2 mg/kg/h, i.v.) and maintained under artificial respiration. The heart rate was monitored, and end-tidal CO_2 concentration and body temperature were maintained at 4% and 38°C, respectively. All incisions were infiltrated with lidocaine. A craniotomy was made bilaterally to expose cortices anterior to the cannula implant sites.

Extracellular recordings were performed with a tungsten microelectrode (4–10 MΩ). A hand-held bar-shaped light stimulus was presented on a screen. OD were evaluated based on a seven-point classification in which the scores 1 and 7 indicate monocular responses to deprived and nondeprived eyes, respectively. A score of 4 indicates equal responses to both eyes and other scores indicate intermediate responses.

Nissl staining

Animals were euthanized with an overdose of sodium pentobarbital and transcardially perfused with cold 20 mM phosphate-buffered saline (PBS, pH 7.4) followed by 4% paraformaldehyde (PFA) in 0.1 M phosphate buffer (PB). Brains were dissected from the skull and postfixed in 4% PFA and 20% sucrose in PB at 4°C. After postfixation, frozen coronal sections (25–50 μm in thickness) were prepared with a microtome (SM2000 R, Leica Biosystems). All sections were mounted on MAS-coated slides (Matsunami Glass Industry), dipped in a 0.2% cresyl violet solution, dehydrated in an ascending series of ethanol, defatted in xylene, and coverslipped with DPX mountant (Merck). Sections were observed with a microscope (ECLIPSE E800M, Nikon) and captured using a cooled CCD camera (VB-7010, KEYENCE). The location of each recording site was determined according to the distance from the electrolytic lesions. Data for neurons located on the layer border were excluded from layer analysis.

Western blotting

Animals were euthanized with an overdose of isoflurane and transcardially perfused with cold 20 mM PBS. Brain tissue was immediately frozen in powdered dry ice. Brains were sliced into 500-μm thick sections using a microtome, and the visual cortex was quickly dissected. The dissected region was confirmed by microscopic observation of residual slices. The tissue was homogenized using a Potter homogenizer with 15 strokes at 3,000 rpm in a homogenizing buffer (0.32 M sucrose, 1 mM EDTA, 1 mM EGTA, and protease inhibitor cocktail (Nacalai Tesque) in 10 mM Tris-HCl (pH 7.4)). The homogenates were centrifuged at 1,000 rpm for 10 min at 4°C and the supernatant was collected. Protein concentration was determined with the Pierce Micro BCA Protein Assay Kit (Thermo Fisher Scientific). The tissue samples were separated by SDS-PAGE and electroblotted onto PVDF membranes. The membranes were blocked with 5% skim milk in 10 mM Tris-buffered saline (pH 7.4) containing 0.1% Tween 20 (T-TBS) and incubated with T-TBS containing one of the following primary antibodies (0.05 μg/ml) overnight at 4°C: rabbit anti-CB1R (AB_2571591, Frontier Institute), rabbit anti-DGLα (AB_2571691, Frontier Institute), or mouse anti-GAPDH antibody (AB_2107445, Merck). The membranes were then incubated with HRP-labeled secondary antibody (1:5,000, donkey anti-rabbit IgG antibody, AB_772206, GE Healthcare; 1:20,000, sheep anti-mouse IgG antibody, AB_772210, GE Healthcare) for 1 hour. The immunoreaction was visualized with an ECL chemiluminescence detection system (ECL plus or ECL prime, GE Healthcare) and digitalized by a CCD imager (LAS-4000, FUJIFILM). Blot densities were quantified using the ImageJ software. All western blot data used for quantification were obtained by applying samples from animals at different postnatal days on the same gel. We have published data on CB1R,[26] and data on GAPDH (Figure 3D) are the same as previous ones.

Immunostaining

Animals were euthanized with an overdose of isoflurane and transcardially perfused with cold PBS (20 mM) followed by 4% PFA in 0.1 M PB. Brains were removed from the skull and postfixed in 4% PFA and 20% sucrose in 0.1M PB overnight at 4°C. Then, frozen coronal sections (30-μm thick) were prepared with a microtome. All immunohistochemical procedures were performed on free-floating sections.

For immunoperoxidase staining, the sections were washed with PBS and incubated in 0.5% H_2O_2 and 0.5% Triton X-100 in PBS for 15 min at room temperature (20–25°C) to block endogenous peroxidase activity. Then, the sections were incubated in a blocking solution (5% normal goat or rabbit serum (Vector Laboratories), 5% bovine serum albumin (BSA) (Merck), and 0.5% Triton X-100 in PBS) at room temperature for 4–5 hours. The sections were reacted with a primary antibody (2 μg/ml, rabbit anti-DGLα antibody) in the blocking solution overnight at 4°C, washed with PBS, incubated with the blocking solution for 4–5 hours, and incubated with the secondary antibody solution (1:200, goat biotinylated anti-rabbit IgG antibody, AB_2313606, Vector Laboratories in blocking solution) overnight at 4°C. They were reacted using the conventional ABC-DAB method. All sections were mounted on MAS-coated slides, dehydrated in an ascending series of ethanol, defatted in xylene, and coverslipped with DPX mountant.

For immunofluorescence, sections were incubated in a blocking solution (5% donkey serum (Jackson ImmunoResearch), 5% BSA, and 0.5% Triton X-100 in PBS or 10% goat serum (Equitech-Bio) and 0.5% Triton X-100 in PBS) for 0.5–2 hours at room temperature. The sections were incubated in the blocking solution containing primary antibodies (2 μg/ml, rabbit anti-DGLα antibody, goat anti-CB1R antibody, AB_2571592, guinea pig anti-CB1R antibody, AB_2571593, rabbit polyclonal anti-$GABA_AR$ α1, AB_2571571, Frontier Institute) overnight at 4°C, washed in PBS, incubated in a secondary antibody (1:200, donkey Alexa 488-conjugated anti-rabbit IgG antibody, AB_2535792, donkey Alexa 568-conjugated anti-goat IgG antibody, AB_2534104, goat Alexa 488-conjugated anti-rabbit IgG antibody, AB_2576217, goat Alexa 647-conjugated anti-guinea pig IgG antibody, AB_2735091, Thermo Fisher Scientific) in blocking solution for 2–3 hours at room temperature. The sections were washed and mounted on MAS-coated slides and coverslipped with Fluoromount/plus (Diagnostic BioSystems).

Slice electrophysiology

We used DGLα-KO and wild-type C57BL/6 mice of either sex at three developmental stages (P15–P17, P20–P22, and P25–P27). Coronal slices, including the primary visual cortex (300-μm thick), were prepared from mice under deep anesthesia with isoflurane. The slices were recovered for 1 hour at 33–34°C in an interface-type chamber perfused with normal artificial cerebrospinal fluid containing the following: 126 mM NaCl, 3 mM KCl, 1.3 mM $MgSO_4$, 2.4 mM $CaCl_2$, 1.2 mM NaH_2PO_4, 26 mM $NaHCO_3$, and 10 mM glucose, saturated with 95% O_2 and 5% CO_2. The slices were then kept in a submerged-type chamber at 24–25°C. Pyramidal-shaped neurons located in layer 2/3 or 4 of the binocular primary visual cortex were targeted by patch pipettes for whole-cell recordings under infrared differential interference contrast optics (BX51, Olympus). Cell bodies of the recorded neurons were located 50 μm below the cut-surface of the slice. The patch pipettes (3–5 MΩ) were filled with an internal solution containing the following: 130 mM Cs-gluconate, 8 mM CsCl, 1 mM $MgCl_2$, 0.6 mM EGTA, 10 mM HEPES, 3 mM MgATP, 0.5 mM Na_2GTP, 10 mM Na-phosphocreatine, and 0.1–0.2% biocytin (pH 7.3 with CsOH). The membrane potentials of recorded neurons were held at 0 mV. mIPSCs were recorded at 24–25°C in the presence of tetrodotoxin (1 μM), the non-NMDA glutamate receptor antagonist NBQX (10 μM), and the NMDA receptor antagonist D-AP5 (50 μM) to block action potentials and glutamatergic excitatory postsynaptic currents. In one part of the experiments, the CB1R inverse agonist AM251 (10 μM) was added. Whole-cell recordings were performed and sampled using Axon Multiclamp 700B amplifier, Digidata 1440A, and pCLAMP10 software (Molecular Devices). Signals were sampled at 10 kHz. Recorded cells with a high seal resistance (>1 GΩ) and a low series resistance <25 MΩ were selected for analysis. The mIPSCs were analyzed using peak analysis software from Synaptosoft and other custom softwares written in MATLAB.

Following the recording, slices were fixed in PBS containing 4% PFA. The slices were resectioned to a thickness of approximately 50 μm. To visualize recorded cell morphology and determine location, slices were incubated in a blocking solution (10% normal goat serum, 0.5% Triton X-100 in 25 mM PBS) at room temperature for 0.5–2 hours. The sections were reacted with a primary antibody (1 μg/ml, rabbit anti-CB1R antibody) in blocking solution overnight at 4°C, washed in PBS, and incubated in a blocking solution that contained the secondary antibody (1:500, goat Alexa 555-conjugated anti-rabbit IgG, AB_2535851, Thermo Fisher Scientific), streptavidin conjugated to Alexa Fluor 488 (1:500; Thermo Fisher Scientific), and DAPI for 2 hours at room temperature. Reconstructed cells in the slice electrophysiological samples were captured by a CCD camera (CX9000, MBF) or confocal microscopy (A1R, Nikon). Pyramidal cells were identified by the morphology of the reconstructed cells. L4 of V1 was determined based on the higher density of DAPI-stained nuclei and weaker immunoreactivity for CB1R than L2/3. The binocular region of V1 was estimated with reference to the boundary between V1 and V2L which was determined based on the weak immunoreactivity for CB1R in L4 of V1.

Data analysis for *in vivo* electrophysiology

Single-unit activity was isolated from the saved data (Offline Sorter, Plexon) and assigned to each stimulus (NeuroExplorer, Nex Technologies). The maximum firing rate during visual stimulation of any direction was defined as the peak response. We used the unit whose peak response was greater than the spontaneous activity for the following analysis. To quantify the OD of each neuron, we calculated the ocular dominance index (ODI) as follows:

$$\mathrm{ODI} = \frac{R_{\mathrm{ipsi}} - R_{\mathrm{contra}}}{R_{\mathrm{ipsi}} + R_{\mathrm{contra}}}$$

where R_{ipsi} and R_{contra} represent the evoked response which is the difference between the peak response and the spontaneous activity to the ipsilateral and contralateral eye, respectively.

When either R_{ipsi} or R_{contra} was ≤ 0, the ODI was calculated with it as 0. In the binocular correspondence experiment, responses during 0.5 s after stimulus presentation were omitted to exclude the effect of ON responses. The orientation selectivity index (OSI) and the angle of the preferred orientation were calculated for each eye using the following equations:

$$\mathrm{OSI} = \frac{\left|\sum R(\theta)\cdot\exp(2i\theta)\right|}{\sum R(\theta)}$$

$$\mathrm{Angle} = \frac{\arg\left(\sum R(\theta)\cdot\exp(2i\theta)\right)}{2}$$

where θ represents the angle of the stimulus and R(θ) is the response to that angle. We selected neurons which satisfied the following conditions in both eyes: peak responses were ≥2.0 spikes/s, peak responses were greater than or equal to two-fold spontaneous activity,

and OSIs were ≥ 0.10. Then, the difference in the preferred angles between the two eyes (ΔO) was calculated to evaluate binocular correspondence.

Image analysis

Image analyses were performed using the ImageJ software. Immunostained sections were captured with a cooled CCD camera. Layer and region boundaries were defined in the neighboring Nissl- or DAPI-stained sections. To measure regional intensities of DGLα, a region of interests (ROI) was set on L2/3 in each region. Then, the mean intensities were calculated and normalized to that in the binocular region. To compare intensity between layers, an ROI (200-μm wide) was set on each layer of the binocular region of V1. Immunoreactive intensities of DGLα were obtained from 12–20 sites of 3–5 animals at each age. The intensity was averaged in each layer, and then normalized to the mean intensity of all layers.

Subcellular localization of DGLα and CB1R

For the subcellular localization of DGLα and CB1R, we used P30 mice. PFA-fixed sections (30-μm thick) were incubated in a blocking solution (5% donkey serum, 5% BSA, and 0.5% Triton X-100 in PBS) for 1–2 hours at room temperature. Then, the sections were incubated in the blocking solution containing primary antibodies (2 μg/ml, rabbit anti-DGLα and goat anti-CB1R) overnight at 4°C, washed in PBS, and incubated in the blocking solution containing biotinylated anti-rabbit IgG antibody (1:500) for 2–3 hours at room temperature. The sections were then processed using the conventional ABC-DAB method for 1 hour at room temperature, washed with PBS, and treated with biotinylated tyramine-glucose oxidase solution for tyramide signal amplification.[61] Then the sections were incubated with Alexa 568-conjugated anti-goat IgG antibody (1:200) and streptavidin conjugated to Alexa Fluor 488 (1:200) for 2 hours at room temperature. Images were acquired with laser confocal microscopy (LSM780, Zeiss) using a 63× oil immersion objective lens (NA = 1.4, Plan-Apo) and stored in 16-bit TIFF file format (4,096 × 4,096 pixels; pixel size = 50 nm). We manually selected varicosity-like structures in CB1R images.[26] We used thresholding at top 4% brightest pixels in the images to obtain DGLα-immunopositive particles. Circular ROIs of various radii centered on a CB1R bouton were created, and the density and size of DGLα particles in each circle were measured.

VEP recording for WIN administered mice

We used wild-type mice at 4 weeks of age. A silver-ball electrode was implanted on the surface of the visual cortex (0.2 mm anterior to the lambda, 3.0 mm to the midline). A head-plate was implanted on the skull and the mice were placed on the stereotaxic apparatus. VEP was measured in an awake state. Signals were amplified and filtered with an AC amplifier (0.1–500 Hz) and digitized at a sampling rate of 1 kHz and stored in a computer. Reversing horizontal square-wave grating patterns (spatial frequency, 0.05 cycle/degree; reversal frequency, 1 Hz) were presented on a display. The stimuli were presented 500 times under binocular condition. The amplitude of VEP was evaluated by the peak-to-trough amplitude during 100 ms after reversing a stimulus. The amplitude of VEP was measured before and 1 hour after WIN administration (5 mg/kg).

QUANTIFICATION AND STATISTICAL ANALYSIS

Statistics

Summarized data of statistics in each figure are presented in Table S1. SPSS or MATLAB software was used for statistical tests. For the electrophysiological experiments, permutation test or Mann–Whitney U-test was used. For the permutation test, rearrangement was performed 1,000 times if the number of all possible combinations exceeds the value. The Holm–Bonferroni correction was used to compare more than two groups. To evaluate results of western blotting and immunostaining, Student's t-test or ANOVA was used. Following ANOVA, Dunnett's post hoc test was performed for multiple comparisons.